Anticlustering of small normal faults around larger faults

Rolf V. Ackermann*
Roy W. Schlische
Department of Geological Sciences, Rutgers University, Busch Campus, Piscataway, New Jersey 08855-1179

ABSTRACT

The Solite quarry in the Mesozoic Danville rift basin contains normal faults that conform to two spatial and size distributions. Larger master normal faults (20 cm < length [*L*] < 200 cm) are not numerous and have spanned the mechanical layer. The other faults are numerous, small (~0.1 cm < *L* < 20 cm), and exhibit anticlustering with respect to the larger structures, defining crack shields around the master faults. The shields are ellipsoidal in shape and geometrically similar to the elastic deformation fields of the master faults, and correspond to a critical stress-reduction shadow that prevented the nucleation of smaller faults in the vicinity of the master faults. The master faults likely formed earlier than the smaller faults, which nucleated en masse when some critical strain threshold was exceeded outside the master fault deformation field. The anticlustered spatial distribution of faults described here is the first field documentation for the existence of stress reduction shadows around normal faults.

INTRODUCTION

Thorough analysis of the spatial distribution of faults is critical to understanding the mechanics and systematics of faulting, fault growth, and fault population evolution. The ability to predict where various structures occur within the volume surrounding a large structure is integral to the construction of fractured aquifer and hydrocarbon reservoir models. Unfortunately, our understanding of the spatial distribution of faults is limited, especially compared to opening-mode fractures (e.g., Gillespie et al., 1993). Some studies have noted that smaller faults cluster around larger faults (e.g., Gauthier and Lake, 1993; Gillespie et al., 1993; Knott et al., 1996; Little, 1996; Watterson et al., 1996). Jackson and White (1989) suggested that very large normal faults in the Basin and Range have a characteristic spacing, but they provide no information on the distribution of smaller scale faults. The spacing of opening-mode fractures changes with increasing strain until the system attains saturation (e.g., Wu and Pollard, 1995), and most studies (see summary in Wu and Pollard, 1995) confirm that the fractures have a characteristic spacing that is proportional to mechanical layer thickness and is governed by a stress-reduction shadow (e.g., Gross et al., 1995), which forms because stress within the rock volume cannot be transmitted across the free surface of the fracture (Gross et al., 1995). Until now, stress shielding between faults has only been casually suggested (e.g., Cowie et al., 1995) or illustrated in numerical models (e.g., Willemse, 1997).

In this paper we report on the spatial distribution of exceptionally well exposed faults from a quarry in the Mesozoic Danville basin in North Carolina. Here, smaller normal faults are clearly anticlustered around larger structures. We argue that this distribution is related to a stress-reduction shadow around the larger faults, and explore the effect of this spatial distribution on the size distribution of faults in the population, the implications for the temporal evolution of this fault system, and the applicability of these concepts to larger scale structures.

POPULATION SYSTEMATICS

The population of small faults is within the Danville rift basin, a half graben that has an east-dipping border fault system. A detailed discussion of the geometry and length-displacement scaling relations of these faults was given in Schlische et al. (1996). These (originally) blind normal faults are readily observed on quarried, clean, bedding-plane partings, permitting detailed spatial analysis. They can also be observed in quarried cross-section exposures, as well as in rock slabs that have been sawed in the lab. All faults have a consistent orientation (045°, 70°SE, bedding corrected) and dip synthetic to the border fault system.

This population can be divided into two broad groups of faults based on size and spatial distribution. Large faults (20 cm < length [*L*] < 200 cm) are infrequent and essentially uniformly distributed throughout the rock volume. Small faults (~0.1 cm < *L* < 20 cm) are generally ubiquitous within the rock volume, but are absent within ellipsoidal regions around the large faults (Fig. 1), which are devoid of brittle structures (in outcrop and thin section). We call these regions crack shields, and use the term shield to distinguish the physical distribution of structures from the mechanical explanation of these features, e.g., stress reduction shadows (Willemse, 1997). Faults surrounded by crack shields are master faults,

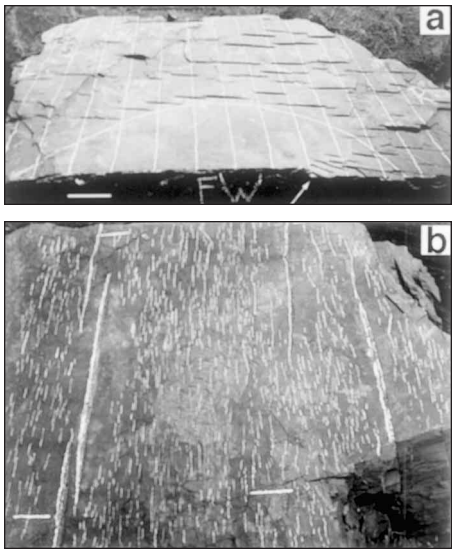

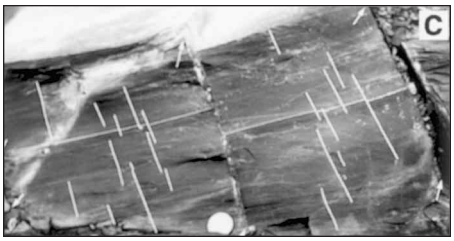

Figure 1. a: Small faults anticlustered around larger normal fault (footwall surface shown in foreground); scale bar in lower left of image is 5 cm. Note breached ramp structure at lower right (arrow). b: Distribution of faults (highlighted) exposed on bedding surface of quarried boulder. Scale bars normal to fault traces are 10 cm. c: Crack shields in cross section; faults are highlighted. Arrows point to tips of master faults. Coin is 2.5 cm wide.

*Present address: Mobil Technology Co., P.O. Box 650232, Dallas, Texas 75265-0232. E-mail: rolf_v_ackermann@email.mobil.com.

regardless of fault size; this is the only basis for master fault definition. Shield geometries vary depending on linkage of larger structures. The smaller faults appear abruptly outside of the crack shields, and there is no increase in the size of the small faults away from the larger structures; rather, they occur in a range of sizes with no apparent systematic variation. The small faults generally follow stepping patterns around master faults: the small faults closest to the master fault change step at the center of the length of the larger structure, as well as at the tips (Fig. 1a). These geometric relationships provide important information about the spatial and temporal evolution of the system, specifically that the larger faults formed and grew first, and then the smaller faults nucleated, most likely with overlapping growth phases.

Faults are generally believed to follow a power-law distribution of sizes such that

$$N = aL^{-C}, \quad (1)$$

where N is number of faults with a length (L) greater than a given size, a is related to the number of faults, and C is the power-law exponent (e.g., Pickering et al., 1995). The power-law exponent gives the ratio of the smallest faults to the largest faults. Thus in populations with larger power-law exponents (steeper slopes), smaller faults are relatively more important in accommodating strain. The power-law exponent is determined by plotting N vs. L on cumulative frequency plots. Typically, such plots are convex upward, consisting of a single central segment (with a slope of $-C$), a shallow upper segment resulting from truncation due to sampling resolution, and a steep lower segment generally ascribed to a censoring effect due to large structures extending out of the sampling area (e.g., Pickering et al., 1995).

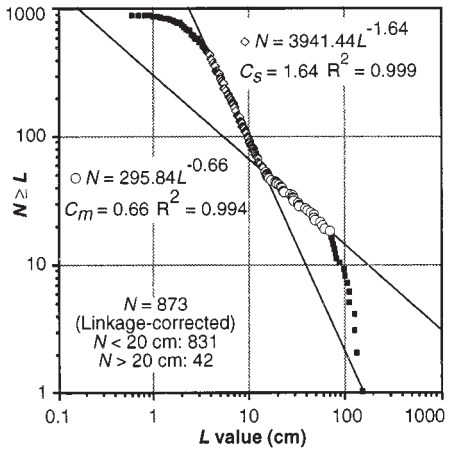

Figure 2. Cumulative frequency (N = number) plot of fault lengths (L) for all structures within ~34 m^2 area. Note two distinct central segments, suggesting two subsets of faults having slopes that differ by ~1.0. Subscripts of m and s are for master faults and small faults, respectively. C is power-law exponent.

Some workers have noted that this simple power-law distribution may not always hold. In particular, Wojtal (1994, 1996) drew attention to fault populations that have faceted central segments, i.e., central portions composed of at least two straight segments with different power-law exponents. Wojtal attributed such faceted diagrams to the effects of fault linkage during the evolution of the population. Despite the faceted appearance, the cumulative frequency plots are still convex upward. In contrast, a cumulative frequency plot (Fig. 2) for faults from the Solite quarry is concave upward and appears to have two central segments, both of which follow a power-law distribution. Figure 2 is based on the distribution of 873 fault lengths measured on a single bedding surface, which were corrected for linkage in the field following Wojtal (1996) and Dawers (1996); the data suffer from truncation and censoring effects.

The two well-defined central segments (Fig. 2) suggest that there are two subpopulations, which in turn reflect the strain history of these rocks. (Removing the master faults from the analysis results in a single central segment nearly identical to the segment covering smaller fault sizes in Fig. 2.) Interestingly, $C_m = 0.66$ for the segment covering the larger fault sizes (master faults), which is ~1 less then that of the other segment ($C_s = 1.64$). Marrett and Allmendinger (1991) observed that the value of C is critically dependent on $f - s$, where f is the geometric dimension of the region occupied by the faults, and s is the sampling dimension. In this example, $s = 2$ (two-dimensional sampling of observed trace lengths) for both subpopulations. The lower value of C_m thus implies that the occupation dimension (f) is lower for the master faults. We suggest that this is because all the faults in the quarry are restricted to discrete mechanical layers (see Ackermann et al., 1996), with the master faults spanning entire layers but not exceeding them. Therefore they occupy only two dimensions ($f = 2$, as opposed to the small faults where $f = 3$); this is analogous to faults that span the brittle crust, which can only grow along strike, having lost one degree of freedom (e.g., equation 2 in Marrett and Allmendinger, 1991). This results in more complete sampling of that subpopulation using a two-dimensional sampling method ($f - s = 0$): all structures will be observed at all structural levels.

Using equations 3–6 from Marrett and Allmendinger (1991) (which account for faults that do and do not span a brittle layer, e.g. $f = 2$ versus $f = 3$), and a value of $n = 1$ (where n is the length-displacement scaling exponent: see Schlische et al., 1996), we calculate B_m (master faults) and B_s (small faults) based on geometric moment (M_g), which is the product of the average displacement and the surface area of the fault (Marrett and Allmendinger, 1991). B is the power-law exponent for the size distribution of M_g, similar to C, and is used here to compare C for subpopulations from the same rock volume, but with different values of f. $B_m = 0.83$ and $B_s = 0.88$, suggesting that the two subpopulations are intricately related, although smaller faults are slightly less important in strain accommodation for the master fault subpopulation. $B_m \approx B_s$ demonstrates that the master faults and the small faults are simply two interrelated components of a single coherent fault population. $C_s - C_m \approx 1$ in turn indicates that one subset of faults has a lower occupation dimension (f) and thus spans the mechanical layer, which is consistent with field observations.

Cumulative frequency plots are commonly used to extrapolate fault size data (following a power-law distribution) measured over a relatively narrow scale range (< three orders of magnitude) in order to estimate the amount of strain accommodated by structures below the sampling resolution (e.g., Marrett and Allmendinger, 1992). The presence of faceted cumulative frequency plots (e.g., Wojtal, 1996) and concave-upward plots (Fig. 2) suggests that such extrapolations should be undertaken with caution.

DEFORMATION FIELDS AND STRESS-REDUCTION SHADOWS

As noted above, the crack shields are approximately ellipsoidal. The size of the ellipsoid is related to fault length and displacement. Figure 3 examines the relationship between displacement along the length of the fault and the distance that the shield projects away from the fault in plan view. Data were collected for eight isolated master faults that have well-defined shields, which were observed at varying structural levels. Projection distances were measured in the field, whereas displacements were calculated using an empirical relationship between distance along the length of the fault and local displacement, derived specifically for this fault population using measured distance-displacement profiles (e.g., Schlische et al., 1996, Fig. 4). The resulting displacement

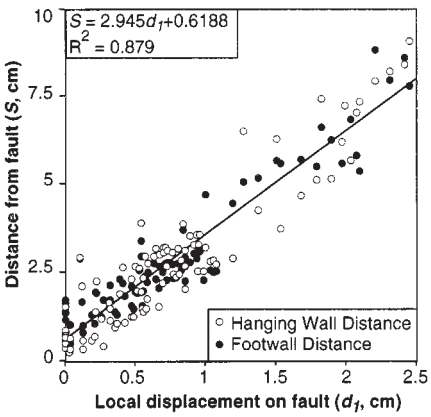

Figure 3. Linear relationship between local displacement (d_1) and crack shield projection distance (S) for master faults from this population.

versus projection distance plot (Fig. 3) shows a well-defined band; deviations above and below the linear curve fit reflect changes in the projection distance that are likely a function of rock properties and different exposure levels on the master faults. This linear relationship is consistent with the documented linear scaling of other fault parameters, such as slip, displacement, breakdown zone size, fracture energy, cataclasite zone width, and process zone wake width with length (Cowie and Scholz, 1992; Scholz, 1990; Vermilye, 1995).

The best-fit curve in Figure 3 allows us to generate an idealized crack shield (Fig. 4), which is geometrically similar to the deformation field associated with normal faults (Gibson et al., 1989). The deformation field includes the displacement discontinuity at the fault surface, the process zone (where inelastic and nonbrittle processes such as plastic deformation, frictional wear, and mechanical breakdown occur at the fault tip; Cowie and Scholz, 1992), and the far-field deformation that affects the volume surrounding the fault (required to maintain geometric coherence; e.g., Barnett et al., 1987). Within the deformation field, strain decreases away from the fault (e.g., Barnett et al., 1987). The deformation field can be modeled by elastic flexure using multiple screw dislocations (see Gupta and Scholz, 1996), although this requires detailed comparison of field data and deflection equations for a specific population. We instead approximate the deformation field by the roll-over radius (R'), defined as the distance perpendicular to the normal fault affected by significant footwall uplift or hanging-wall subsidence, expressed as:

$$R' = R'_{max}\left(\frac{d}{d_{max}}\right)^{1/2} \quad (2)$$

where d is the displacement on the fault, and d_{max} is the maximum displacement. R'_{max} is the maximum roll-over radius, taken to be equal to the mean of the major and minor radii of the fault surface ellipse; axial ratios of normal faults generally range from 1.25 to 3 (Gibson et al., 1989). Use of this equation is consistent with Willemse's (1997) model of the influence of fault shape on the distribution of stress and strain around a normal fault; the geometry produced in Figure 4 is nearly identical to that in Figure 5 of Willemse (1997).

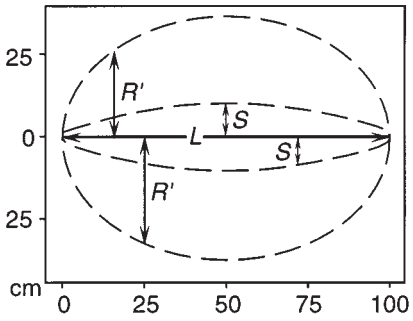

Figure 4. Map view of simple model for relationship between deformation field and crack shield at the center of isolated, blind, normal fault. Extent of crack shield will vary with rock properties and strain rate, and terminates where stress locally exceeds shear strength of rock. R' = roll-over radius, L = length (100 cm), S = crack shield projection distance, d_{max} = 3 cm, axial ratio = 2 (Gupta and Scholz, 1996).

Geometrically, the crack shield and the deformation field for a 1-m-long fault are similar, although the shield is about one-quarter the predicted size of the deformation field (Fig. 4). Because the deformation field represents a volume of rock in which the material has been relaxed (strained), it should be a proxy for a stress-reduction shadow around a fault (e.g., Willemse, 1997). The crack shield therefore occupies a part of the stress-reduction shadow, specifically that portion where the stress did not exceed the shear strength of the rock. Thus, it would be possible to have brittle failure within the deformation field of a fault but not in the volume in the immediate vicinity of the fault, the size of which is governed by the size of the fault and material properties; strain rate is likely to be important as well, as discussed below.

The interpretation that the crack shields correspond to a critical stress-reduction shadow is consistent with the Willemse (1997) model, bolstered by the almost complete absence of brittle structures within the crack shields. The idealized crack shield shown in Figure 4 lies within the region of highest stress-reduction associated with slip on a fault (Willemse, 1997, Fig. 5). In addition to calculating areas that have undergone stress-reduction, the Willemse (1997) model predicts regions that undergo an increase in stress. The highest stresses are found near the tips of the faults. This may lead to the preferential development of smaller faults in these areas, some of which may be incorporated into the process zone as the fault tips propagate during growth. The higher density of faults in these areas may also explain why some authors have reported clustering of smaller faults near larger faults (e.g., Gauthier and Lake, 1993; Gillespie et al., 1993; Knott et al., 1996; Little, 1996; Watterson et al., 1996). We note that our crack shield geometries break down in areas where master faults have linked together; prior to linkage, these areas may have had higher numbers of smaller faults surrounding the fault tips.

DISCUSSION

The two distinct subsets of the fault population in the Solite quarry provide specific information about the spatial and temporal evolution of this population. We interpret the deformation history here as follows: (1) A set of faults formed from random flaws within the rock volume in response to a remote applied stress (Triassic rifting). These grew and linked through time, elastically interacting at both short and long ranges (see also Cowie et al., 1995; Willemse, 1997). Given the variable sizes of the master faults, it is unlikely that they all nucleated at the same time. Rather, new faults continued to nucleate while older faults grew, some of which linked together. The younger faults probably continued to nucleate at random flaws, the only constraint being that younger faults would not nucleate in the crack shields of the older faults. (2) At some point, an elastic threshold was exceeded within the rock volume, perhaps related to the amount of elastic shear strain that can be accommodated prior to brittle failure, or corresponding to the stage when the tips of the master faults reached mechanical layer boundaries. At that point, the original set of faults was no longer sufficient to accommodate the strain, which necessitated the mass nucleation of a second set of faults. However, the deformation fields/stress-reduction shadows of the original set of faults governed the spatial distribution of the new faults so that they did not form within regions surrounding the larger structures where either the stress was not great enough to exceed the shear strength of the rock, or elastic strain accommodation was sufficient enough such that an elastic threshold was not exceeded. Thus the smaller faults are relatively late stage features, although they formed over multiple slip events (Schlische et al., 1996).

The system discussed here is simpler than the majority of systems studied, which are of much larger scale. However, because many of the features and processes of faults and fault growth are scale invariant (e.g., Cowie and Scholz, 1992; Schlische et al., 1996), and because much of the deformation associated with faulting in the Earth's crust is elastic at all scales (e.g., Gupta and Scholz, 1996; Willemse, 1997), the analysis of these crack shields provides important insights into faulting at all scales. It may be that stress-reduction shadows and crack shields can only be observed at small scales, at low strains, in simple settings. At larger scales and strains, it may not be possible to accommodate all of the strain in the deformation field elastically; loading, erosion, and isostasy provide additional complications. Nonetheless, it may be that even large fault zones are surrounded by some region that is less deformed, or that shows a radial increase in fault size, which formed as the stress-reduction shadow of the larger structure slowly engulfed and deactivated smaller structures as it grew through time.

Eventually, the largest faults will grow to such a size that they completely cut through a mechanical layer (whether it is a single sedimentary layer or the brittle crust). In the absence of bedding parallel detachments (such as at the Solite quarry; Ackermann et al., 1996) these large faults will no longer propagate up-dip and down-dip, but will continue to propagate along strike (as opposed to the intrablock rotation of Gross et al., 1997). The effect of this is that the ellipticity

of the fault surface will increase, and the displacement profile will change from bell-shaped to flat-topped (see Dawers et al., 1993); increased rates of along-strike propagation may lead to an increase in lateral fault linkage. Because the crack shield/stress-reduction shadow scales with displacement, and because the maximum displacement no longer increases significantly once the fault has broken through a mechanical layer, the end result of this evolutionary scenario is a series of large faults with a quasiregular spacing, which itself is a function of mechanical layer thickness, maximum displacements, and stress-reduction shadows (this scenario is similar to that for opening-mode fractures; Wu and Pollard, 1995). As noted in the introduction, the large basin-bounding faults in the Basin and Range have a characteristic spacing that Jackson and White (1989) speculated was a function of the thickness of the seismogenic layer.

In summary, the exceptionally well-exposed population of small faults in the Solite quarry provides an opportunity for detailed spatial, temporal, and kinematic analyses. The results of these analyses suggest that there are two discrete yet closely related subsets to this particular population, and, more important, suggest the existence of stress-reduction shadows around normal faults. In this example, remnants of the shadows have been preserved as crack shields around larger structures that are devoid of mesoscopic and microscopic faults. We suggest that the spatial distribution of normal faults is governed by stress-reduction shadows approximated by the deformation fields of these structures, the rate of stress recovery away from the fault (governed by rock properties), and the short- and long-range elastic interaction between faults (e.g., Cowie et al., 1995; Willemse, 1997).

ACKNOWLEDGMENTS

We thank C. H. Gover and the Virginia Solite Corporation for their support of this research. Financial support was provided by Mobil Corporation, the Rutgers Research Council, and the Virginia Museum of Natural History. Valuable insights and/or field assistance were provided by J. Carpenter, P. Cowie, N. Dawers, G. Eisenstadt, P. Hennings, A. Gupta, K. Meisling, P. Olsen, C. Scholz, B. Shaw, and M. Withjack. We appreciate the thorough and constructive reviews by D. Pollard and S. Wojtal.

REFERENCES

Ackermann, R. V., Johnson, L. A., Patiño, L. C., and Schlische, R. W., 1996, Fracture partitioning in the Cow Branch Formation, Danville rift basin: Influence of mechanical stratigraphy on Mohr-Coulomb failure: Geological Society of America Abstracts with Programs, v. 28, no. 3, p. 33.

Barnett, J. A. M., Mortimer, J., Rippon, J. H., Walsh, J. J., and Watterson, J., 1987, Displacement geometry in the volume containing a single normal fault: American Association of Petroleum Geologists Bulletin, v. 71, p. 925–937.

Cowie, P. A., and Scholz, C. H., 1992, Physical explanation for displacement-length relationship of faults using a post-yield fracture mechanics model: Journal of Structural Geology, v. 14, p. 1133–1148.

Cowie, P. A., Sornette, D., and Vanneste, C., 1995, Multifractal scaling properties of a growing fault population: Geophysical Journal International, v. 122, p. 457–469.

Dawers, N. H., Anders, M. H., and Scholz, C. H., 1993, Growth of normal faults: Displacement-length scaling: Geology, v. 21, p. 1107–1110.

Dawers, N. H., 1996, Fault size distribution on the Volcanic Tableland, California: Implications for small-scale fault prediction, *in* Faulting, fault sealing and fluid flow in hydrocarbon reservoirs: University of Leeds Rock Deformation Research Group, in conjunction with the Petroleum Group & Tectonic Studies Group, Geological Society of London, Abstract, p. 88–89.

Gauthier, B. M., and Lake, S. D., 1993, Probabilistic modeling of faults below the limit of seismic resolution in Pelican Field, North Sea, United Kingdom: American Association of Petroleum Geologists Bulletin, v. 77, p. 761–777.

Gibson, J. R., Walsh, J. J., and Watterson, J., 1989, Modelling of bed contours and cross-sections adjacent to planar normal faults: Journal of Structural Geology, v. 11, p. 317–328.

Gillespie, P. A., Howard, C. B., Walsh, J. J., and Watterson, J., 1993, Measurement and characterization of spatial distributions of fractures: Tectonophysics, v. 226, p. 113–141.

Gross, M. R., Fischer, M. P., Engelder, T., and Greenfield, R. J., 1995, Factors controlling joint spacing in interbedded sedimentary rocks: Integrating numerical models with field observations from the Monterey Formation, USA, *in* Ameen, M. S., ed., Fractography: Fracture topography as a tool in fracture mechanics and stress analysis: Geological Society of London Special Publication 92, p. 215–233.

Gross, M. R., Gutiérrez-Alonso, G., Bai, T., Wacker, M. A., and Collinsworth, K. B., 1997, Influence of mechanical stratigraphy and kinematics on fault scaling relations: Journal of Structural Geology, v. 19, p. 171–183.

Gupta, A., and Scholz, C. H., 1996, Validity of elastic models in predicting fault displacement fields: Eos (Transactions, American Geophysical Union), v. 77, supplement, p. 484.

Jackson, J. A., and White, N. J., 1989, Normal faulting in the upper continental crust: Observations from regions of active extension: Journal of Structural Geology, v. 11, p. 15–36.

Knott, S. D., Beach, A., Brockbank, P. J., Brown, J. L., McCallum, J. E., and Welbon, A. I., 1996, Spatial and mechanical controls on normal fault populations: Journal of Structural Geology, v. 18, p. 359–372.

Little, T. A., 1996, Faulting-related displacement gradients and strain adjacent to the Awatere strike-slip fault in New Zealand: Journal of Structural Geology, v. 18, p. 321–340.

Marrett, R., and Allmendinger, R. W., 1991, Estimates of strain due to brittle faulting: Sampling fault populations: Journal of Structural Geology, v. 13, p. 735–738.

Marrett, R., and Allmendinger, R. W., 1992, Amount of extension on "small" faults: An example from the Viking graben: Geology, v. 20, p. 47–50.

Pickering, G., Bull, J. M., and Sanderson, D. J., 1995, Sampling power-law distributions: Tectonophysics, v. 248, p. 1–20.

Schlische, R. W., Young, S. S., Ackermann, R. V., and Gupta, A., 1996, Geometry and scaling relations of a population of very small rift-related normal faults: Geology, v. 24, p. 683–686.

Scholz, C. H., 1990, The mechanics of earthquakes and faulting: New York, Cambridge University Press, 439 p.

Vermilye, J., 1995, The process zone: A fracture mechanics interpretation: Eos (Transactions, American Geophysical Union), v. 76, supplement, p. 565.

Watterson, J., Walsh, J. J., Gillespie, P. A., and Easton, S., 1996, Scaling systematics of fault sizes on a large scale range fault map: Journal of Structural Geology, v. 18, p. 199–214.

Willemse, E. J. M., 1997, Segmented normal faults: Correspondence between three-dimensional mechanical models and field data: Journal of Geophysical Research, v. 102, p. 675–692.

Wojtal, S. F., 1994, Fault scaling laws and the temporal evolution of fault systems: Journal of Structural Geology, v. 16, p. 603–612.

Wojtal, S. F., 1996, Changes in fault displacement populations correlated to linkage between faults: Journal of Structural Geology, v. 18, p. 265–280.

Wu, H., and Pollard, D. D., 1995, An experimental study of the relationship between joint spacing and layer thickness: Journal of Structural Geology, v. 17, p. 887–905.

Manuscript received April 4, 1997
Revised manuscript received September 16, 1997
Manuscript accepted September 23, 1997